Bio-FET Sensor Interface Module for COVID-19 Monitoring Using IoT

https://doi.org/10.3991/ijoe.v18i12.31877

Govind Maniam[1], Jahariah Sampe[1(✉)], Rosmina Jaafar[1], Azrul Azlan Hamzah[1], Noraziah Mohamad Zin[2]
[1]Universiti Kebangsaan Malaysia (UKM), Bangi, Selangor, Malaysia
[2]Universiti Kebangsaan Malaysia (UKM), Kuala Lumpur, Malaysia
jahariah@ukm.edu.my

Abstract—Rapid transmission of the coronavirus disease via droplets and particles has led to a global pandemic. Expeditious detection of SARS-Cov-2 RNA in the environment is attainable by using Bio-FET sensors. This work proposes a Bio-FET sensor interface module with IoT implementation to amplify signals from a Bio-FET for SARS-Cov-2 detection and monitoring. The sensor interface module was programmed to read the signals using a micro-controller and process information to determine the presence of SARS-Cov-2. The proposed Bio-FET sensor interface module was also set to transmit data to the Cloud via W-Fi to be stored and displayed on a dashboard. The prototype Bio-FET sensor interface module was simulated in PSpice for signal amplification, and hardware implementation has been done by using low-cost components for data transmission to the Cloud. The hardware consists of an AD620 instrumentation amplifier module, voltage sensor module, Neo-6m GPS sensor module, an OLED display, and an ESP8266-32 bit micro-controller. The results of both the simulation and the hardware implementation are similar. The emulated negative and positive Bio-FET signal outputs were successfully amplified from 15.9mV and 45.8mV to 1.59V and 4.58V, respectively, using an AD620 instrumentation amplifier. The gathered location, time, date, output voltage, and SARS-Cov-2 presence results were successfully stored and displayed on the Cloud dashboard.

Keywords—Bio-FET, Internet of Things, COVID-19, biosensor, cloud

1 Introduction

Coronavirus disease (COVID -19) is a dangerous infectious disease also knows as SARS-CoV-2. COVID-19 was first discovered in the city of Wuhan in December 2019 [1]. This virus is set to target the respiratory organs of humans, causing them to have breathing difficulties and, in worst scenarios, organ damages and death. COVID-19 affects people of all ages, increasing the risk of infection in the young and the elderly. The transmission of the COVID-19 virus is through respiratory droplets via the mouth or nose. The virus spreads when an infected human coughs, sneeze or talks causing the adjacent humans to get infected. The Centers for Disease Control

and Prevention (CDC) has discovered new COVID-19 variants [2]. As of now, there are five COVID-19 variants out around the world. The most recent variants are the Delta and Omicron variants. These emerging variants spread the virus faster and cause severe symptoms upon infection [3]. The SARS-Cov-2 RNA has an incubation period of 6 to 7 days [4]. The incubation period, known as the interval between initial infection and onset of disease. Hence, an infected human will only notice the COVID-19 symptoms after the incubation period. The probability of SARS-Cov-2 transmission is higher when an infected person shows symptoms to the virus [5].

Many efforts were undertaken in the early stages of the COVID-19 pandemic to keep the pandemic from becoming worse than it was. Research has been done to determine the cause, symptoms and ways of detecting COVID-19 in humans. One of the earliest breakthroughs was made to detect COVID-19 in humans using test kits [6]. Test kits, namely Reverse Transcription Polymerase Chain Reaction (RT-PCR) and Antigen Rapid Test Kit (RTK-Ag), were made by pharmaceutical companies to identify COVID-19 infections. Medical professionals handled these test kits on people testing to see if the virus infected them. These test kits played a significant role during the COVID-19 pandemic to avoid transmitting the virus. Patients were kept quarantined after a positive COVID-19 result while the area of the infected person is fumigated to kill the virus on common surfaces. This proves to be an ingenious method to stop the spread of SARS-Cov-2 RNA in environment as infected humans tend to unintentionally transmit SARS-Cov-2 RNA via contact, droplets and aerosols before they are diagnosed [7].

A faster and more efficient detection method can be done by using field-effect transistors (FET) as biosensors to detect infectious diseases. These sensors are also known as biosensor field-effect transistors (Bio-FET) [8]. Bio-FET is known to be producing rapid and accurate results in detecting specific viruses when modified with different materials [9]. Common materials are graphene, reduced graphene oxide (rGo), and titanium oxide [10]. A Bio-FET sensor consists of a source metal, drain metal and a semiconducting layer with a bio-sensitive layer known as a gate [11]. Figure 1 shows a Bio-FET sensor that is used for the detection of infectious diseases. The Bio-FET sensor has a source, drain and gate electrode that produces signals electrically. This allows possible implementation of Internet of Things (IoT) using a micro-controller for remote real-time monitoring of COVID-19 in the environment.

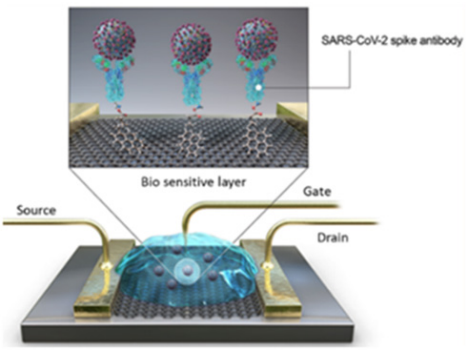

Fig. 1. Bio-FET sensor [9]

Wireless Sensor Network (WSN) has been more commonly used in monitoring systems involving IoT. WSN are low powered interconnected sensors linked wirelessly to collect information about the surrounding environment [12]–[14]. Countless monitoring systems are being developed to monitor multiple parameters at the same time. Interconnecting multiple sensors to collect data simultaneously will allow more accurate environmental monitoring [15]–[17]. For instance, E-Health monitoring systems are currently being studied to prevent people from attaining contagious diseases or even chronic diseases [18]–[21].

This research shows a high degree of innovation in terms of combining IoT with Bio-FET sensors to detect various infectious diseases. There has been a wide range of research on incorporating IoT to detect pollution in the environment, such as air quality and water pollution. However, very little research has been done to use IoT for detecting and monitoring viral contamination such as COVID-19 in the environment. These Bio-FET sensor interface modules can be used in a multitude of applications. The sensor interface module can be used to develop devices that can be placed around buildings for constant monitoring. Highly concentrated areas like hospitals, schools or offices can utilize the developed device to detect the presence of SARS-Cov-2 in the environment. In another instance, organizers conducting events could deploy these developed devices across the event venue to detect and monitor the presence of the COVID-19 virus. On detection, the attendees of the event can take precautionary measures to quarantine or take a COVID-19 test. Furthermore, the device prototype hardware is developed using low-cost components, making it both economical and simple to discard in the event of viral contamination. The device prototype's cost-effectiveness also enables the installation of large numbers of modules in numerous locations for improved detection and monitoring. Finally, this device is user-friendly since it is simple to operate and can be used by people of all ages. The device can be set up without the assistance of healthcare professionals or technicians.

2 Literature review

Airborne SARS CoV-2 RNA is commonly transmitted via droplets or aerosols based on particle size and aerodynamic diameter. Particles larger than 5 m are classified as droplets, whereas those less than 5 m are classified as aerosols or droplet nuclei [22]. Droplet transmission occurs when an infected patient coughs, speaks, or sneezes and sprays big droplets onto the conjunctiva or mucous membranes of a vulnerable host. Meanwhile, contact transmission can occur through direct physical contact between an infected individual and a vulnerable host, as well as indirect contact with infectious secretions on fomites. Research comparing the aerosol and surface stability of SARS-CoV-2 and SARS-CoV-1 found that both viruses had similar surface stability [23]. The three-hour-long experiment shows SARS-CoV-2 remained viable in aerosols throughout the duration. The infectious titer of SARS-CoV-2 in aerosols decreased from $10^{3.5}$ to $10^{2.7}$ 50% tissue-culture infectious dose ($TCID_{50}$) per liter of air while identical drop is seen with SARS-CoV-1 when $TCID_{50}$ per milliliter decreased from $10^{4.3}$ to$10^{3.5}$. The study also reported that SARS-CoV-2 can remain active in the air for several hours, posing a risk of aerosolized transmission.

Table 1 shows the surface stability data of SARS-CoV-2 on different materials [24]. The half-life of SARS-CoV-2 on stainless steel was 2.26−17.9 hours, 2.26−15.33 hours on ABS plastic, and 2.26−15.33 hours on nitrile gloves. This concludes no significant difference in viral persistence based on surface. The half-life of SARS-CoV-2 was found to reduce as temperature and humidity gained across all three materials.

Table 1. Surface stability data using SARS-CoV-2 with >3 samples/surface and half-life end point [24]

Material	Humidity	Temperature (°C)	Half-Life (Hours)
Stainless steel	30–40	4–30	9.10–17.90
	20–80	24–35	2.26–15.33
ABS Plastic	20–80	24–35	2.26–15.33
Nitrile Gloves	20–60	24–35	2.26–15.33

The detection of surface contamination and airborne SARS-CoV-2 can be done several ways. The detection of SARS-CoV-2 on surfaces has been done by collecting samples using scrub contact prone surface with a wet cotton swab. Then, the swab is immersed in 3 mL of sodium chloride solution or a buffer solution. Finally, the sample is tested using RT-PCR or RT-qPCR [25], [26]. The sampling of airborne SARS-CoV-2 using an air pump using a constant flow rate. The air samples will be collected using pre-sterilized gelatin filters (Sartorius) [27]. A similar method of scrubbing contact prone surfaces has been done in hospitals to further understand the severity level of SARS-CoV-2 transmission. Similar sampling method has been done on a study conducted by the University of Nebraska Medical Center [28]. The findings confirm viral contamination among all surface samples collected. The samples were collected in 13 different rooms of confirmed positive patients. To add on, 70.6% of all personal items sampled were determined to be positive.

A study to detect airborne SARS-CoV-2 has been done at two hospitals in Wuhan [27]. Results show that the concentration of SARS-CoV-2 RNA in aerosols detected in isolation wards and ventilated patient rooms was deficient. Still, it was higher in the toilet areas used by the patients. A similar test conducted by the University of Nebraska Medical Center has found that 63.2% of in-room air samples to be positive by RT-PCR [28]. Another study to detect SARS-CoV-2 RNA in aerosols was conducted in three of the air samples including those collected using a robot-assisted sampler were detected positive by a digital PCR with a concentration level of 9–219 viruses/m^3. This studies mention further verification of SARS-Cov-2 RNA transmission through aerosols and surface contamination. Rapid detection of SARS-Cov-2 RNA has been studied for faster and more accurate virus detection. Bio-FET is introduced to achieve this goal [29]. In a recent study, graphene-based Bio-FET sensors are deemed to have fast response time and accuracy in detecting SARS-Cov-2 [30]. Table 2 shows the performance comparison of previously developed graphene-based field effect transistors for detection method, the limit of detection (LoD), detection range, and time required to generate final test. The Bio-FET sensors are capable to detect the SARS-Cov-2 RNA with LoD down to femtogram (fg) with relatively rapid response time.

Table 2. Performance comparison of previously developed graphene based Bio-FET

Detection Method	LoD	Detection Range	Detection Time	Ref
CNT-FET	5.5fg/mL	5.5fg/mL to 5.5pg/mL	2 min	[31]
Graphene-FET	1fg/mL	1fg/mL to 10pg/mL	5–8 min	[9]
Graphite electrode functionalized with AuNPs-cys	229fg/mL	1pg/mL to 1ng/mL	6.5 min	[32]
CNT-FET	4.12fg/mL	0.1fg/mL to 5.0pg/mL	2–3 min	[29]

Recent research in Korea has concluded that a graphene-based FET sensor is capable to detect SARS CoV-2 virus accurately [9]. The G-FET biosensor was exposed to MERS-CoV and the SARS CoV-2 viruses. As a result, the G-FET biosensor correctly responded when exposed to the SARS Cov-2 virus, proving the accuracy of a Bio-FET sensor to detect a specific virus. The reference outputs of a Bio-FET sensors was taken from an existing developed sensor. This Bio-FET sensor used the gate voltage (V_g) to receive its response signal on detection of SARS-Cov-2 [33]. Figure 2 shows the response of the gate voltage at the charge neutrality point (V_{CNP}) of a Bio-FET sensor when tested COVID-19 samples taken from confirmed positive and negative COVID-19 patients [33]. 20 COVID-19 positive patients (red) and 10 healthy samples (green) were exposed to the Bio-FET sensor. The findings show that healthy samples give an output signal below 30mV, whereas COVID-19 Positive samples gave an output signal of more than 30mV. Thus, concluding the threshold of SARS CoV-2 detection more or equal to 30mV to be considered as positive.

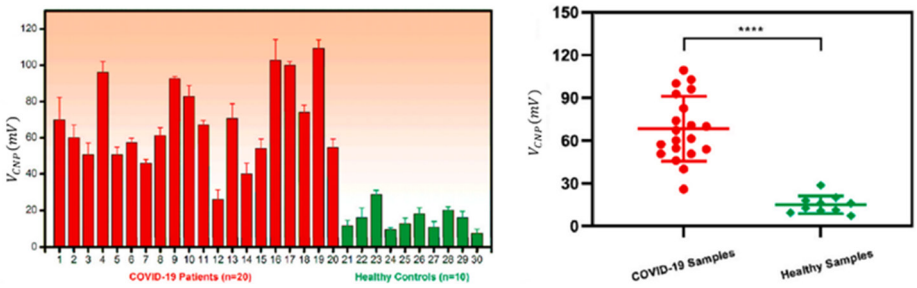

Fig. 2. Bio-FET sensor gate voltage reading against COVID-19 positive patients' samples and healthy samples [33]

3 Proposed Bio-FET sensor interface module

The change in the V_{CYP} is the most widely utilised electrical measure in a graphene-based Bio-FET sensor, depending on whether the graphene is p-doped or n-doped. Intrinsic graphene with low drain-source bias is deduced at values near 0V [34]. However, V_{CNP} can be positive or negative depending on whether the graphene is p-doped or n-doped. Contact between biological targets and biorecognition structures on graphene's surface can modify the material's doping state, leading to a change in the initial V_{CNP} value. As a result, the initial output voltage of the Bio-FET sensor is not 0V.

Readout circuits are used to measure the V_{CNP} of the Bio-FET sensor. The most common readout circuits used are non-differential measurements in a Constant-Voltage Constant-Current configuration [8]. The current and drain voltage of Bio-FETs remain constant, whereas the source voltage varies depending on whether SARS-Cov-2 is detected. The readout circuit of the Bio-FET sensor interface module consists of an amplifier and a voltage sensor module.

Referring to Figure 2, the output voltage range at the gate, V_{CNP}, is from 1mV to 120mV. The ultra-low voltage of the Bio-FET sensor's output could not be measured because the microcontroller's voltage reading threshold is 1.0V. Thus, signal processing is required in the readout circuit to ensure that the microcontroller can read the input values. Signal processing block consists of amplifiers and voltage sensor modules [35], [36]. The Bio-FET sensor's output signal will be amplified using an instrumentation amplifier module [37], [38]. The instrumentation amplifier circuit has three Operational Amplifiers (op-amp) to obtain a gain of 100 purposely for amplifying the input voltage from mV to V. Figure 3 shows the circuit diagram of the classic three op-amp amplification circuit in a non-inverting configuration. The input (V_{in}) is connected to the non-inverting terminal and a simple voltage divider is connected to the inverting terminal for signal amplification. Op-amps 1 and 2 are non-inverting amplifiers, while op-amp 3 is a difference amplifier, forming an instrumentation amplifier. The instrumentation amplifier's final output, V_{out}, is the amplified difference of the input signals applied to the input terminals of op-amp 3.

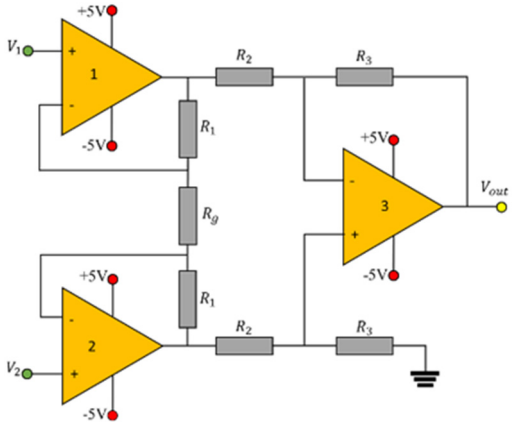

Fig. 3. Three op-amp instrumentation amplifier circuit

Equation (1) represents the formula to calculate the gain of the three op-amp instrumentation amplifier circuit.

$$A = \frac{V_{out}}{V_2 - V_1} \tag{1}$$

Where A represents gain, V_{out} is the output of the amplifier circuit and V_2, V_1 is the differential input of the amplifier circuit. Then equation (2), is used to calculate the output of the amplifier circuit.

$$V_{out} = (V_2 - V_1)\left[1 + \left(\frac{2R_1}{R_g}\right)\right]\left(\frac{R_3}{R_2}\right) \tag{2}$$

Where, V_{out} represents the output of the instrumentation amplifier, V_1, V_2 is the defferential input of the amplifier circuit, R_g is the gain resistor used to determine the gain and R_1, R_2 and R_3 are pairs of resistors having the same value. The the op-amp amplifier circuit has many components that make it complex and frail.

Off-the-shelf amplifier modules were sought to provide a simple yet robust technique for reading out the Bio-FET signals. The amplifier module must amplify the signals while maintaining a 0V initial output voltage measurement. Following further examination, it was found that the AD620 instrumentation amplifier module was the most viable solution for addressing these criteria. The AD620 instrumentation amplifier is a low-cost monolithic instrumentation amplifier based on a modification of the classic three op-amp approach. It can amplify inputs as low as 1.0μV and operate with a voltage supply as low as 5V.

The AD620 instrumentation amplifier module has two LM358 op-amps. The LM358 connected to the *Ref* pin of the AD620 is used to correct the zero error of the output using a variable resistor (Zero). Thus, ensuring a initial voltage readout of 0V. Another LM358 is placed at the output of the AD620 to act as a voltage follower. The voltage follower is added to improve the signal impedance. The gain of the AD620 is controlled by a 10kΩ variable resistor, R_g, placed at pins 1 and 8. This allows the module to have a gain of 1.5 to 1000 without any signal loss. The gain of the AD620 is calculated using equation 3.

$$A = \frac{49.4k\Omega}{R_g} + 1 \tag{3}$$

Where A is the gain and R_g is the value of the variable resistor. The internal gain resistor of the AD620 is trimmed to an absolute value of 49.4kΩ. To obtain a gain of 100, the R_g is set to 499Ω.

The proposed Bio-FET sensor interface prototype's input signal amplification was simulated using PSpice. The AD620 instrumentation amplifier and the LM358 operational amplifiers were used to run the simulation. The circuit was designed referring to the AD620 instrumentation amplifier module that was chosen. Figure 4 shows the PSpice simulation model of the AD620 instrumentation amplifier module. The AD620 and the LM358 have been given a 5V DC power supply to realistically imitate the Bio-FET sensor interface module, which the micro-controller will supply. The reference pin of the simulated AD620 is grounded as the LM358 op-amp connected to the reference pin in the module is only to adjust the zero error that may occur in the device.

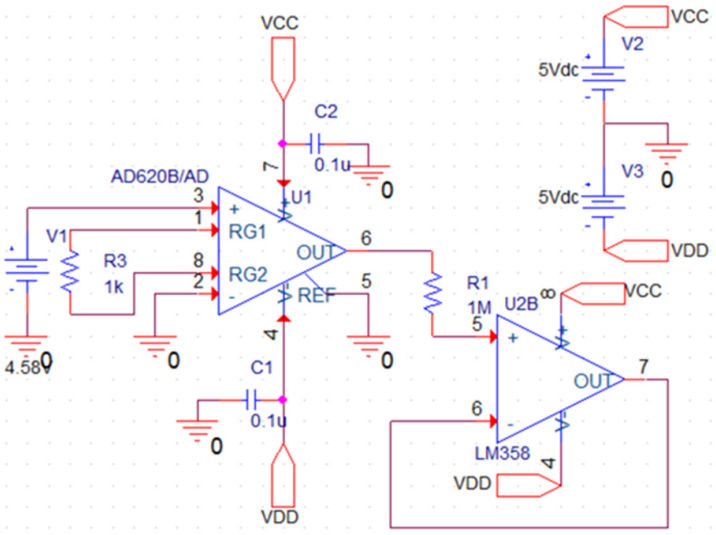

Fig. 4. PSpice simulation model of AD620 instrumentation amplifier module

The signals will go through a voltage sensor module after the amplification process. The voltage sensor module uses a voltage divider principle to measure voltage. The voltage sensor module will give out an analog signal that will go through the built-in Analog to Digital Converter (ADC) of the micro-controller unit. The micro-controller will be programmed to justify the presence of SARS-Cov-2 RNA using the threshold voltage (V_{th}) that is set. The V_{th} was set to 3.00V, thus, if the voltage sensed by the voltage sensor module is below 3.00V, then the results will be displayed as negative portraying no presence of SARS-Cov-2 RNA. Otherwise, if a voltage more than 3.00V is measured, the results will be positive detection of SARS-Cov-2 RNA. This device is set to house 2 Bio-FET sensors that operate simultaneously. The values of the Bio-FET sensors will be individually read and displayed on the OLED display and the Cloud.

The Bio-FET sensor's signal processing capabilities are extended using Internet of Things (IoT) to make a smart Bio-FET sensor interface module. This module is able to send the results to a Cloud database including date, time, and location information simultaneously. Figure 5 shows the steps in signal processing for the intelligent Bio-FET sensor interface module.

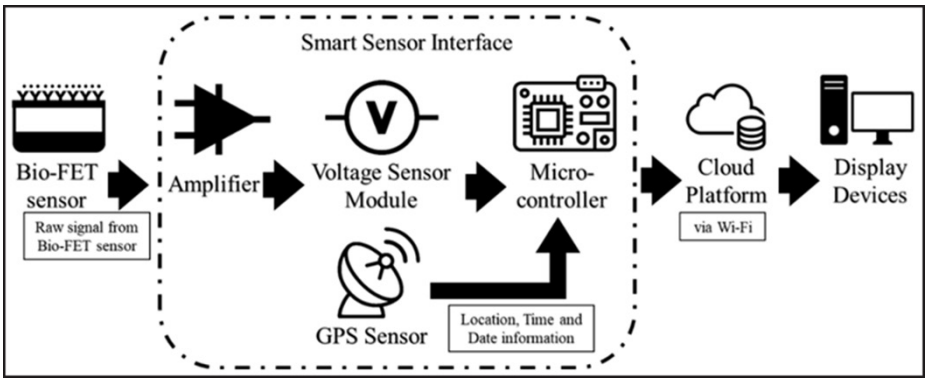

Fig. 5. Proposed Bio-FET sensor interface module

The smart sensor interface module includes the amplifier circuit, voltage sensor module, GPS sensor and the micro-controller unit. The newly added GPS sensor will collect the date, time and location data from nearby satellites. The information provided by the GPS sensor will be read by the micro-controller unit. The micro-controller unit is the brain of the module. The micro-controller functions to collect data from the voltage sensor module and the GPS sensor and send it to the Cloud platform via Wi-Fi connectivity. The micro-controller will also justify the Bio-FET sensor output to determine the detection of SARS-Cov-2 RNA in the environment. The results of the SARS-Cov-2 RNA and the module's location will also be displayed locally on the module itself. In addition, the cloud platform will store the data and display it on devices like personal computers or smartphones.

4 Hardware implementation of Bio-FET sensor interface module

Hardware implementation has been done for the proposed Bio-FET sensor interface module. The Bio-FET sensor interface module has several components that emulate the complete device. It consists of an AD620 instrumentation amplifier module and a voltage sensor module for signal processing. It also has a Neo-6m GPS module developed by ©u-blox to obtain location coordinates and an OLED display to show the results locally. The ESP8266 32-bit micro-controller unit houses all the sensors including the display unit.

The AD620 instrumentation module was used to amplify output signals from the Bio-FET sensor. The amplifier has the capability to amplify DC voltage as low as 1μV and has a gain of 1 to 1000. The AD620 sensor is commonly used in bio-medical devices to amplify ultra-low powered devices. Then, the voltage sensor module is used to detect the voltage at the output of the AD620 instrumentation amplifier. The voltage sensor has an analog output connected to the analog pins of the ESP8266 micro-controller.

Next is the Neo-6m GPS module. The GPS module is placed in the device to provide location services to the user. The Neo-6m is capable of collecting date, time, and location data accurately from multiple satellites simultaneously. The data is then transmitted to the micro-controller using the transmitter and receiver pins. Next, the OLED displays the results with a 128x64 pixel display. The OLED display used is a low-powered device with supplied 3.3V until 5.0V. The OLED display is integrated with an I^2C interface that only uses 2 pins allowing fewer wires to be connected to the micro-controller. Finally, the ESP8266 32-bit micro-controller collects the data from the sensors, displays it locally, and sends it to the Cloud. It has a built-in Wi-Fi module, I^2C interface protocol and analog to digital converter (ADC). The ADC is useful to convert the analog signals from the voltage sensor module to digital signals. Other than that, the built-in Wi-Fi module allows easy access to the Cloud. The I^2C interface protocol allows the OLED display to be connected with minimal wiring. All the sensors can be powered using the 5V output supply of the ESP8266. The ESP8266 has 6 analog input pins that allows multiple Bio-FET sensors to be read by micro-controller simultaneously. Figure 6 shows the hardware implementation of the proposed Bio-FET sensor interface module.

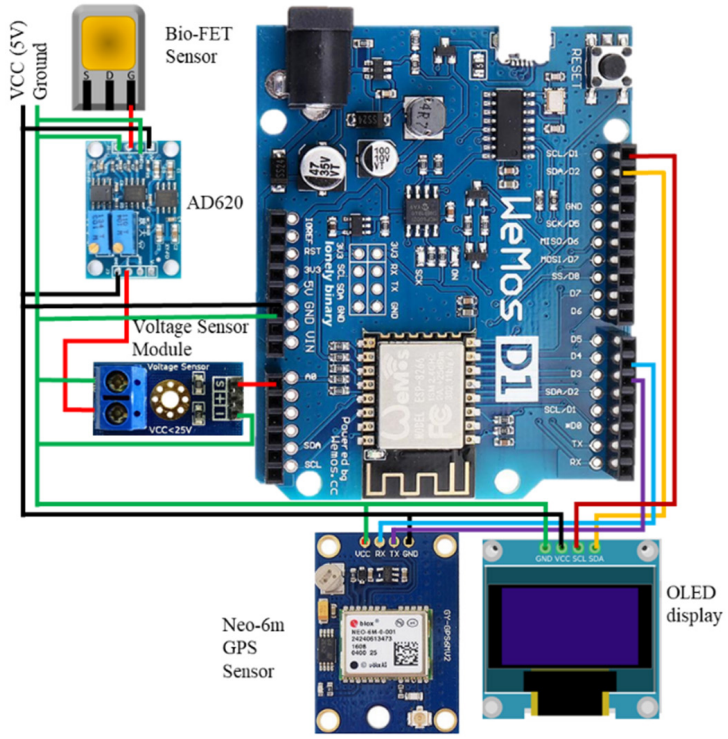

Fig. 6. Hardware implementation of Bio-FET sensor interface module

The gate voltage of the Bio-FET sensor is attached to the S+ pin of the AD620 instrumentation amplifier. The instrumentation amplifier is powered using a 5V supply from the ESP8266 micro-controller by attaching the 5V pin and GND pin of the micro-controller to the V+ and V- pins of the AD620 instrumentation amplifier module. The outputs of the AD620 is connected to the input of the voltage sensor module. The V_{out} and GND of the AD620 are connected to the VCC and GND pins of the voltage sensor module, respectively. The voltage sensor module is also powered using the 5V supply of the ESP8266. The output of the voltage sensor module (S) is connected to the analog pin A0 of the micro-controller. The proposed Bio-FET sensor interface module is intended to read multiple sensors simultaneously. In regards to that, this prototype is housed with another Bio-FET sensor with its own instrumentation amplifier and a voltage sensor module connected pin A1of the micro-controller. This results in two bio-FET sensor readings to be obtained simultaneously.

```
void sensorInfo(){
int value0 = analogRead(Sensorpin0);
double voltage0 = map(value0, 0, 1024, 0, 2500);
voltage0/= 100;
int value1 = analogRead(Sensorpin1);
double voltage1 = map(value1, 0, 1024, 0, 2500);
voltage1/= 100; }
```

Next is the Neo-6m GPS module. The transmitter (TX) and the receiver (RX) of the micro-controller are first declared in the coding of the micro-controller. Here, digital pin 4 is declared as TX and digital pin 3 is declared as RX. Then, the wiring is done with a cross pattern, with the TX of the GPS module connected to the RX of the micro-controller and RX of the GPS module connected to the TX of the micro-controller. The GPS sensor module is also powered using the 5V supply from the micro-controller. Finally, The SDA and SDL pin of the OLED display is connected to the SDA and SCL pins of the ESP8266, respectively.

The proposed device prototype has been programmed using the Arduino Integrated Development Environment (IDE). The Arduino IDE is a software used to program onto micro-controllers which are also known as sketches written on a coding editor. Figure 7 shows the flowchart for the programming written using the C++ language. The Bio-FET sensor interface module was coded as follows: on starting the device, the micro-controller is programmed to initialize the sensors that connected to it. The output voltages from sensors 1 and 2 are read by using analog pin A0 and A1, respectively. The TX and RX pins of the ESP8266 32-bit micro-controller has been declared to digital pin 4 and 3, respectively. Finally, the built-in Wi-Fi module is declared along with the username and password of the Wi-Fi modem that will connect to. The device will then proceed to connect to the Internet and Cloud platform. When the internet is connected, it will try to login onto the Cloud. This step will repeat when a failure occurs. With a successful connection, the micro-controller is programmed to get the sensor readings and the GPS coordinates. The "if statement" is utilized to conclude if the gate voltage of the Bio-FET sensor is over or under the threshold that has been set.

```
if (voltage0 > 3.00) {
    results0 =positiveRed;
  } else {
    results0 =negativeGreen; }

if (voltage1 > 3.00) {
    results1 =positiveRed;
  } else {
    results1 =negativeGreen; }
```

The OLED display will then display the voltage readings of the Bio-FET sensor gate voltage as well as the result and the location of the sensor. The results displayed on the OLED will also be sent to the Cloud platform for remote monitoring and data storage. Unless the device is switched off, the micro-controller will continue reading the data from the sensors and send it to the Cloud. The cloud platform chosen for this prototype is the Arduino IoT Cloud. This cloud platform provides many services such as data displaying using dashboards, data storage, unlimited sensor variables, and a smartphone application run on Android and iOS.

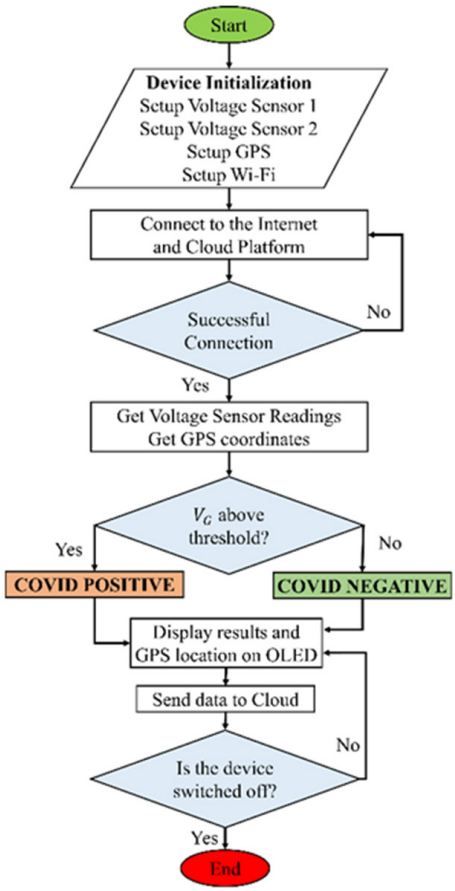

Fig. 7. Operation flowchart of Bio-FET interface sensor module

5 Results and discussion

Results are yielded from the PSpice simulation, hardware implementation and the Cloud platform. The results are compared to ensure the viability of the proposed Bio-FET sensor interface module.

Figure 8 shows the results of the simulation done on the AD620 instrumentation amplifier module to amplify the output signals of the Bio-FET sensor. The x-axis represents the input voltage of the simulated AD620 is referred from output voltage of the Bio-FET sensor in Figure 2. The input voltage range set at the Bio-FET output voltage is from 1 to 120mV. The y-axis represents the output of the simulated AD620 instrumentation module. Referring to the same Bio-FET sensor, V_{th} is set at 30mV, resulting in an output of 3.00V. The rail-to-rail output of the instrumentation amplifier module allows the output voltage to reach saturation at 4.98V with an input voltage of 49mV. Thus, allowing the AD620 instrumentation amplifier module to be applicable as V_{th} is achieved before saturation occurs.

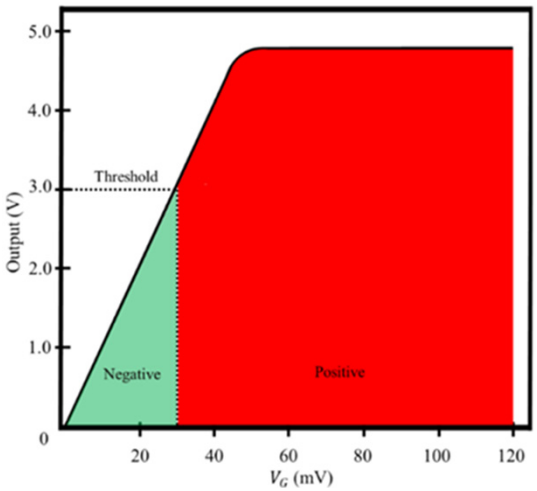

Fig. 8. Output of amplification circuit against Bio-FET sensor output voltage

The proposed Bio-FET sensor interface module prototype hardware was tested using an mV power supply to verify the simulation results. The inputs of the AD620 instrumentation amplifier was supplied with voltage in the range of 1–120mV. Figure 9 shows the OLED display of the proposed Bio-FET sensor interface module prototype. The first and second line of the OLED display shows the longitude and latitude of the device. The longitude is 2.91####, and the latitude is 101.77####. Line 3 and 4 show the Bio-FET sensor readings for Sensors 1 and 2. Sensor 1 and Sensor 2 was supplied with 15.9mV and 45.8mV, respectively. On the OLED display's third line, the amplified voltage sensor readings are displayed on the OLED as 1.59V and 4.58V for Sensor 1 and Sensor 2, respectively. The final line of the OLED display shows the result of the readings. Sensor 1 is "Negative" as the voltage is less than the V_{th}, and sensor 2 is "Positive" as it is more than the V_{th}. Subsequently, the input voltage at the AD620

instrumentation amplifier was increased to 60mv, 80mV and 100mV. However, the output voltage maintains at 5.00V, proving the instrumentation amplifier reached its saturation point, similar to the PSpice simulation results.

Fig. 9. Proposed Bio-FET sensor interface module OLED display

The results displayed on the OLED is similarly displayed on the smartphone Application of the Arduino IoT Cloud. Figure 10 shows the interface of the Arduino IoT Smartphone Application. Sensor 1 and Sensor 2 show 1.59V and 4.58V, respectively. Sensor 1 displays a green mark indicating a negative result, while Sensor 2 displays a red mark indicating a positive result. The results of the sensors shown on the smartphone application are similar to the results displayed on the OLED display. To add on, there is also a map on the smartphone application pointing out the device's location at the same point displayed on the OLED display. Finally, the GPS coordinates sent to the Cloud has successfully plotted on a map on the dashboard. The map displayed on the phone points out the laboratory's location.

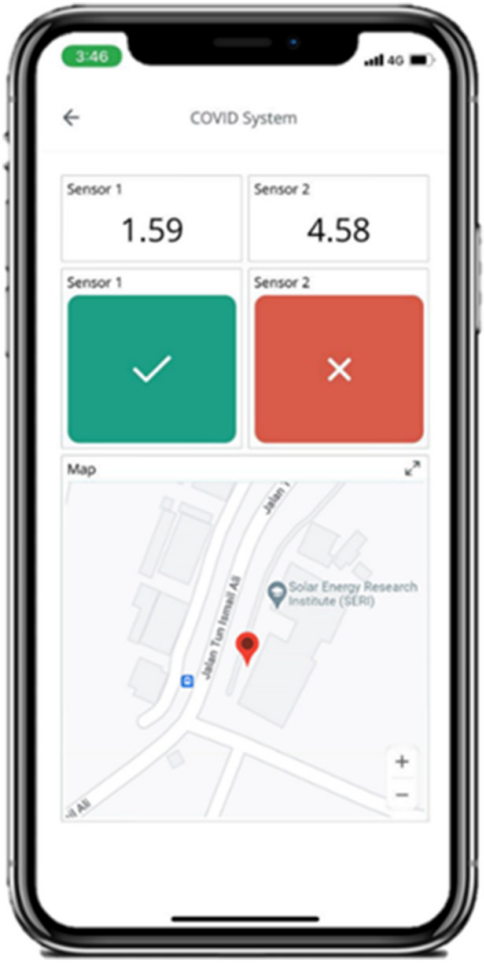

Fig. 10. Smartphone application interface for cloud

6 Conclusion

A Bio-FET sensor interface module prototype was designed to detect SARS-Cov-2 RNA in the environment. The sensor interface module is also equipped with a GPS sensor for accurately locating the device and Wi-Fi module for connectivity with the Cloud. Results of the proposed simulation model has been proven to be valid when compared with the data from the hardware implementation results. The hardware implementation was tested by using mV power supply to imitate the Bio-FET sensor. The Bio-FET signals was successfully amplified from 15.9mV and 45.8mV to 1.59V

and 4.58V respectively. The micro-controller was able to identify the presence of SAR-Cov-2 RNA using the amplified signals. All the data read by the micro-controller was successfully transmitter to the Cloud platform for real-time monitoring and data storage.

7 Acknowledgment

This work is funded by Ministry of Education Malaysia under the grants (UKM-TR-014) and FRGS/1/2018/TK04/UKM/02/1.

8 References

[1] Y. Jin et al., "Virology, epidemiology, pathogenesis, and control of covid-19," Viruses, vol. 12, no. 4, pp. 1–17, 2020, https://doi.org/10.3390/v12040372

[2] S. E. Smith-Jeffcoat et al., "Multistate outbreak of SARS-CoV-2 B.1.1.529 (Omicron) variant infections among persons in a social network attending a convention – New York City, November 18–December 20, 2021," MMWR. Morb. Mortal. Wkly. Rep., vol. 71, no. 7, pp. 238–242, 2022, https://doi.org/10.15585/mmwr.mm7107a3

[3] I. Nemet et al., "Effectiveness of BNT162b2 vaccine against omicron variant in South Africa," N. Engl. J. Med., vol. 386, no. 5, pp. 492–494, 2022, https://doi.org/10.1056/NEJMc2119358

[4] C. Cheng et al., "The incubation period of COVID-19: A global meta-analysis of 53 studies and a Chinese observation study of 11 545 patients," Infect. Dis. Poverty, vol. 10, no. 1, pp. 1–13, 2021, https://doi.org/10.1186/s40249-021-00901-9

[5] A. Agrawal and R. Bhardwaj, "Probability of COVID-19 infection by cough of a normal person and a super-spreader," Phys. Fluids, vol. 031704, pp. 1–7, 2021, https://doi.org/10.1063/5.0041596

[6] M. E. El Zowalaty and J. D. Järhult, "From SARS to COVID-19: A previously unknown SARS- related coronavirus (SARS-CoV-2) of pandemic potential infecting humans – Call for a one health approach," One Heal., vol. 9, no. February, p. 100124, 2020, https://doi.org/10.1016/j.onehlt.2020.100124

[7] Y. C. Wu, C. S. Chen, and Y. J. Chan, "The outbreak of COVID-19: An overview," J. Chinese Med. Assoc., vol. 83, no. 3, pp. 217–220, 2020, https://doi.org/10.1097/JCMA.0000000000000270

[8] A. Panahi, D. Sadighbayan, S. Forouhi, and E. Ghafar-Zadeh, "Recent advances of field-effect transistor technology for infectious diseases," Biosensors, vol. 11, no. 4, 2021, https://doi.org/10.3390/bios11040103

[9] G. Seo et al., "Rapid detection of COVID-19 causative virus (SARS-CoV-2) in Human Nasopharyngeal Swab Specimens using Field-Effect Transistor-Based Biosensor," ACS Nano, vol. 14, no. 4, pp. 5135–5142, 2020, https://doi.org/10.1021/acsnano.0c02823

[10] J. Sengupta and C. M. Hussain, "Graphene-based field-effect transistor biosensors for the rapid detection and analysis of viruses: A perspective in view of COVID-19," Carbon Trends, vol. 2, p. 100011, 2021, https://doi.org/10.1016/j.cartre.2020.100011

[11] D. Sung and J. Koo, "A review of BioFET's basic principles and materials for biomedical applications," Biomed. Eng. Lett., vol. 11, no. 2, pp. 85–96, 2021, https://doi.org/10.1007/s13534-021-00187-8

[12] F. Mohammad, J. Sampe, S. Shireen, and S. Hamid Md Ali, "Minimum passive components based lossy and lossless inductor simulators employing a new active block," AEU – Int. J. Electron. Commun., vol. 82, pp. 226–240, 2017, https://doi.org/10.1016/j.aeue.2017.08.046

[13] M. Faseehuddin, J. Sampe, and S. Shireen, "Lossy and lossless inductance simulators and universal filters employing a new versatile active block," J. Microelectron. Electron. Components Mater., vol. 48, no. 2, pp. 97–113, 2018.

[14] L. Ge, Q. Wang, P. Hu, Z. Hu, and J. B. Liao, "Method of wireless sensor network node deployment for the emergency environment," Int. J. online Biomed. Eng., vol. 13, no. 8, pp. 163–173, 2017, https://doi.org/10.3991/ijoe.v13i08.7422

[15] J. Sampe, M. Faseehuddin, and S. H. M. Ali, "Design of ultra-low voltage CCII utilizing level shifting technique and a dual mode multifunction universal filter as an application," J. Eng. Res., vol. 6, no. 2, pp. 155–175, 2018.

[16] N. H. Mohd Yunus, J. Sampe, J. Yunas, A. Pawi, and Z. A. Rhazali, "MEMS based antenna of energy harvester for wireless sensor node," Microsyst. Technol., vol. 26, no. 9, pp. 2785–2792, 2020, https://doi.org/10.1007/s00542-020-04842-5

[17] T. N. T. Mohamad, J. Sampe, and D. D. Berhanuddin, "RF and thermal hybrid input for ultra-low power semi-active UHF RFID tags," Proc. – 2018 IEEE 14th Int. Colloq. Signal Process. its Appl. CSPA 2018, no. March, pp. 47–51, 2018, https://doi.org/10.1109/CSPA.2018.8368683

[18] G. Maniam, J. Sampe, A. A. Hamzah, M. Faseehuddin, and Noorhidayah, "Biosensor interface controller for chronic kidney disease monitoring using Internet of Things (IoT)," J. Phys. Conf. Ser., vol. 1933, no. 1, 2021, https://doi.org/10.1088/1742-6596/1933/1/012110

[19] G. Maniam and J. Sampe, "Smart monitoring system for chronic kidney disease patients based on fuzzy logic and IoT," vol. 13, no. 2, pp. 324–333, 2022, https://doi.org/10.14569/IJACSA.2022.0130238

[20] M. M. Abdellatif and W. Mohamed, "Telemedicine: An IoT based remote healthcare system," Int. J. online Biomed. Eng., vol. 16, no. 6, pp. 72–81, 2020, https://doi.org/10.3991/ijoe.v16i06.13651

[21] M. Pandurski and F. Tsvetanov, "Application of Sensor Networks for Measuring Insulin Levels," Int. J. online Biomed. Eng., vol. 16, no. 4, pp. 122–136, 2020, https://doi.org/10.3991/ijoe.v16i14.17185

[22] J. D. Siegel, E. Rhinehart, M. Jackson, L. Chiarello, and the Healthcare Infection Control Practices Advisory Committee, "Guideline for Isolation Precautions: Preventing Transmission of Infectious Agents in Healthcare Settings," Centers Diasease Control Prev., pp. 1–232, 2019, [Online]. Available: https://www.cdc.gov/infectioncontrol/pdf/guidelines/isolation-guidelines-H.pdf

[23] V. Doremalen, "Aerosol and surface stability of SARS-CoV-2 as compared with SARS-CoV-1," N. Engl. J. Med., pp. 0–2, 2020, https://doi.org/10.1101/2020.03.09.20033217

[24] J. Biryukov et al., "Increasing temperature and relative humidity accelerates inactivation of SARS-CoV-2 on surfaces," mSphere, vol. 5, no. 4, pp. 1–9, 2020, https://doi.org/10.1128/mSphere.00441-20

[25] L. Zhou et al., "Breath-, air- and surface-borne SARS-CoV-2 in hospitals," J. Aerosol Sci., vol. 152, no. October 2020, pp. 4–10, 2021, https://doi.org/10.1016/j.jaerosci.2020.105693

[26] B. Wan et al., "On-site analysis of COVID-19 on the surfaces in wards," Sci. Total Environ., vol. 753, no. 865, p. 141758, 2021, https://doi.org/10.1016/j.scitotenv.2020.141758

[27] Y. Liu et al., "Aerodynamic analysis of SARS-CoV-2 in two Wuhan hospitals," Nature, vol. 582, no. 7813, pp. 557–560, 2020, https://doi.org/10.1038/s41586-020-2271-3

[28] J. L. Santarpia et al., "Aerosol and surface contamination of SARS-CoV-2 observed in quarantine and isolation care," Sci. Rep., vol. 10, no. 1, pp. 1–8, 2020, https://doi.org/10.1038/s41598-020-69286-3

[29] M. A. Zamzami et al., "Carbon nanotube field-effect transistor (CNT-FET)-based biosensor for rapid detection of SARS-CoV-2 (COVID-19) surface spike protein S1," Bioelectrochemistry, vol. 143, p. 107982, 2022, https://doi.org/10.1016/j.bioelechem.2021.107982
[30] S. Afroj, L. Britnell, T. Hasan, D. V. Andreeva, K. S. Novoselov, and N. Karim, "Graphene-based technologies for tackling COVID-19 and future pandemics," Adv. Funct. Mater., vol. 31, no. 52, 2021, https://doi.org/10.1002/adfm.202107407
[31] W. Shao, M. R. Shurin, S. E. Wheeler, X. He, and A. Star, "Rapid detection of SARS-CoV-2 antigens using high-purity semiconducting single-walled carbon nanotube-based field-effect transistors," ACS Appl. Mater. Interfaces, vol. 13, no. 8, pp. 10321–10327, 2021, https://doi.org/10.1021/acsami.0c22589
[32] L. F. de Lima, A. L. Ferreira, M. D. T. Torres, W. R. de Araujo, and C. de la Fuente-Nunez, "Minute-scale detection of SARS-CoV-2 using a low-cost biosensor composed of pencil graphite electrodes," Proc. Natl. Acad. Sci. U. S. A., vol. 118, no. 30, pp. 1–9, 2021, https://doi.org/10.1073/pnas.2106724118
[33] J. Li et al., "Rapid and unamplified identification of COVID-19 with morpholino-modified graphene field-effect transistor nanosensor," Biosens. Bioelectron., vol. 183, no. December 2020, 2021, https://doi.org/10.1016/j.bios.2021.113206
[34] A. Béraud, M. Sauvage, C. M. Bazán, M. Tie, A. Bencherif, and D. Bouilly, "Graphene field-effect transistors as bioanalytical sensors: Design, operation and performance," Analyst, vol. 146, no. 2, pp. 403–428, 2021, https://doi.org/10.1039/D0AN01661F
[35] M. Faseehuddin, N. Herencsar, M. A. Albrni, and J. Sampe, "Electronically tunable mixed-mode universal filter employing a single active block and a minimum number of passive components," Appl. Sci., vol. 11, no. 1, pp. 1–26, 2021, https://doi.org/10.3390/app11010055
[36] M. Ibharim, A. Albrni, F. Mohammad, N. Herencsar, J. Sampe, and S. H. Ali, "Novel electronically tunable biquadratic mixed-mode universal filter capable of operating in MISO and SIMO configurations," J. Microelectron. Electron. Components Mater., vol. 50, no. 3, pp. 189–203, 2020.
[37] N. A. A. Semsudin, J. Sampe, M. S. Islam, A. R. M. Zain, and D. D. Berhanuddin, "Designing a boost converter of micro energy harvester using thermal and vibration input for biomedical devices," RSM 2015 – 2015 IEEE Reg. Symp. Micro Nano Electron. Proc., pp. 8–11, 2015, https://doi.org/10.1109/RSM.2015.7354974
[38] F. F. Zulkifli, J. Sampe, M. S. Islam, M. A. Mohamed, and S. A. Wahab, "Optimization of RF-DC converter in micro energy harvester using voltage boosting network and bulk modulation technique for biomedical devices," RSM 2015 – 2015 IEEE Reg. Symp. Micro Nano Electron. Proc., pp. 8–11, 2015, https://doi.org/10.1109/RSM.2015.7354975

9 Authors

Govind Maniam is a postgraduate student at the Institute of Microengineering and Nanoelectronics at Universiti Kebangsaan Malaysia. His research interests are biomedical system design and Internet of Things.

Ir. Dr. Jahariah Sampe is a senior lecturer at the Institute of Microengineering and Nanoelectronics at Universiti Kebangsaan Malaysia. Her research interest includes VLSI design, MEMS, ultra-low powered energy harvesters and biomedical devices.

Dr. Rosmina Jaafar is a senior lecturer at the Dept. Electrical, Electronics & Systems Engineering Faculty of Engineering & Built Environment at Universiti Kebangsaan Malaysia. Her research interest are signal processing, imaging and medical informatics as well as medical electronics & instrumentation.

Prof. Dr. Azrul Azlan Hamzah is the director of the Institute of Microengineering and Nanoelectronics at Universiti Kebangsaan Malaysia. His research interests are MEMS design, NEMS, biomedical systems, and biosensors.

Prof. Dr. Noraziah Mohamad Zin is a senior lecturer in the Faculty of Health Sciences at Universiti Kebangsaan Malaysia. Her research interests are anti infection from microbial metabolites, antimicrobial resistance and infectious diseases in communities.

Article submitted 2022-04-21. Resubmitted 2022-06-03. Final acceptance 2022-06-03. Final version published as submitted by the authors.